[CANCER RESEARCH 60, 2541–2546, May 1, 2000]

Temporal Progression of Metastasis in Lung: Cell Survival, Dormancy, and Location Dependence of Metastatic Inefficiency[1]

M. Dianne Cameron, Eric E. Schmidt,[2] Nancy Kerkvliet, Kishore V. Nadkarni, Vincent L. Morris, Alan C. Groom, Ann F. Chambers,[3] and Ian C. MacDonald

Departments of Medical Biophysics [M. D. C., E. E. S., K. V. N., V. L. M., A. C. G., A. F. C., I. C. M.], Microbiology and Immunology [V. L. M., A. F. C.], and Oncology [V. L. M., A. F. C.], University of Western Ontario, and London Regional Cancer Centre [N. K., A. F. C.], London, Ontario, Canada N6A 4L6

ABSTRACT

Cancer metastasis is an inefficient process. The steps in metastasis responsible for this inefficiency and how metastatic inefficiency can vary in different locations within an organ remain poorly understood. B16F10 cells were injected to target mouse lung, and at sequential times thereafter we quantified in lung the time course of: (*a*) overall cell survival and metastatic development; and (*b*) local cell survival and growth with respect to the lung surface and specific interior structures. We found high rates of initial survival of cells trapped in the lung circulation, extravasation into lung tissue, and subsequent survival of extravasated solitary cells (74% at day 3) before metastasis formation. However, at the time of initial replication of metastatic cells a major loss of cells occurred. Although only a small proportion of injected cells started to form metastases, most of these developed into macroscopic tumors. Solitary cells found at later times were dormant. Thus, overall metastatic inefficiency was largely due to postextravasation events affecting solitary cells. Regionally within the lung, cells and metastases were randomly distributed to day 4, but by day 10 preferential tumor growth was found along the lung surface and around arterial and venous vessels. Thus, trapping and early growth of injected cells was unaffected by location within the lung, whereas subsequent metastatic growth was enhanced in specific microenvironments. This study: (*a*) quantifies early temporal and spatial progression of metastasis in lung; (*b*) documents persistence of solitary dormant cells; and (*c*) shows that metastatic inefficiency depends on the initiation of growth in a subset of extravasated cells, whereas continued growth of metastases occurs preferentially in specific tissue environments.

INTRODUCTION

Metastasis is the foremost cause of death from cancer (1–3). Fortunately, metastasis is an extremely inefficient process (4), with few of the many cells shed from a primary tumor successfully forming secondary tumors. It is, thus, important to understand what happens to cancer cells between their entry into the circulation and the formation of metastases. Some cell loss may occur in the circulation due to hemodynamic forces (5) or the immune system (6, 7), but our studies in both chick embryo CAM[4] and mouse liver (8, 9) have shown that >80% of injected melanoma cells can survive initial arrest in the microcirculation and extravasate. These findings suggest that metastatic inefficiency was due primarily to events that occurred after extravasation. In mouse liver, we quantified the survival of B16F1 melanoma cells at successive stages of the metastatic process after extravasation and identified two key contributors to metastatic inefficiency in that model: only 1 in 40 cells initiated growth, and only 1 in 100 early micrometastases continued to grow into macroscopic tumors, whereas the rest disappeared (9). Because this has been the only study of its kind in any organ, it remains unknown whether the rate-limiting steps we identified also apply to other cells and organs.

Metastatic inefficiency may also vary depending on location within an organ. In mouse liver, extravasated rhabdomyosarcoma cells have been shown to migrate to the subcapsular region before cell division begins (10, 11), and the majority of metastases are located at the surface rather than in the interior (9, 12). Moreover, when migration to the surface is inhibited, there is a corresponding decrease in number of metastatic foci (11). In chick CAM (the respiratory organ of the embryo), most extravasated murine melanoma cells migrate preferentially to arterioles, wrap around them, and replicate there (13, 14).

In mouse, it has been reported that cancer cells injected into the tail vein arrive via the blood stream at random distances from the outer surface of the lung, but metastases are located primarily at the surface or near major structures in the interior, 2 weeks after injection (15–17). It is not known, however, whether this preferential distribution is due to destruction of solitary cells at some sites before growth begins, initiation of cell division at preferred sites, or continued growth only at preferred sites. Because the lung is the first organ encountered by cells from most primary tumors after entering the bloodstream (except for those entering the splanchnic circulation), it is a particularly vulnerable site for metastasis. It is, therefore, important to determine the rate-limiting steps affecting overall cancer cell survival and growth in lung and also those locations in the lung that affect metastatic inefficiency.

The two objectives of this study were: (*a*) to quantify overall tumor cell survival and growth over time during metastatsis development in mouse lung; and (*b*) to quantify the initial distribution and survival of individual cancer cells within the lung, as well as the initiation and continuation of cancer cell growth, in relation to the lung surface and major interior structures. By identifying the locations of cells and metastases at successive times after i.v. injection, we could determine whether a selective distribution of tumors within the organ resulted from preferential (*a*) initial distribution of cells, (*b*) cell survival, (*c*) initial growth to form microscopic tumors, or (*d*) continued growth to form visible tumors at specific sites.

We determined the survival of B16F10 melanoma cells in mouse lung at sequential time points, from initial arrest in the microcirculation up to 14 days later. An accounting technique using reference microspheres (8, 9) was used to quantify survival of solitary cells, small metastases, and macroscopic tumors. At early times (to day 4), the spatial distributions of cells and small metastases relative to the lung surface or major structures in the interior (arteries, veins, and bronchioles ≥ 100 μm) were determined by computer analysis of digitized images of thick sections, whereas immunohistochemistry of thin sections was used to assess apoptosis (TUNEL) and proliferation (Ki-67) in solitary cells and metastases. For later times, the proportion of tumor tissue adjacent to specific lung structures was assessed. Our results showed that throughout the metastatic process survival of injected cells in the lung is much greater than previously thought. Furthermore, the initial distribution of injected cells is uniform cells throughout the lung, and their survival and initial growth are inde-

Received 10/25/99; accepted 3/3/00.

The costs of publication of this article were defrayed in part by the payment of page charges. This article must therefore be hereby marked *advertisement* in accordance with 18 U.S.C. Section 1734 solely to indicate this fact.

[1] Supported by National Cancer Institute of Canada Grant 8133.

[2] Deceased, August 19, 1999.

[3] To whom requests for reprints should be addressed, at London Regional Cancer Centre, 790 Commissioners Road East, London, Ontario, Canada N6A 4L6. Phone: (519) 685-8652; Fax: (519) 685-8646; E-mail: ann.chambers@lrcc.on.ca.

[4] The abbreviations used are: CAM, chorioallantoic membrane; TUNEL, terminal deoxynucleotidyl transferase-mediated nick end labeling.

pendent of location, whereas continued growth of early metastases occurs at selective sites.

MATERIALS AND METHODS

Cell Culture and Labeling

B16F10 murine melanoma cells were grown in α-MEM with added ribonucleosides (α-plus MEM; Life Technologies, Inc., Burlington, Ontario, Canada) plus 10% FCS (Hyclone Laboratories, Logan, UT). Subconfluent monolayers (70–80% confluency) were subcultured every 3 days and were not maintained in culture beyond four passages. To positively identify cells within the lung tissue, they were labeled before injection with fluorescent nanospheres (Fluoresbrite 48-nm diameter; Polysciences, Warrington, PA), as described (10). The nanospheres remain brightly visible within intact cells and dim only as diluted by cell division. Plating efficiency and growth curve experiments verified that labeled cells remained viable with unimpaired growth *in vitro*. For injection, cells were trypsinized and resuspended in α-plus MEM/10% FCS; more than 95% of the cells excluded ethidium bromide, indicating that membrane integrity was maintained (18, 19). Finally, 9-μm diameter fluorescent microspheres (Bangs Laboratories Inc., Fishers, IN) were added to the cell suspension (cells:microspheres $\simeq$5:1) for monitoring of cell survival using the cell accounting procedure given below.

Animal Preparation

Female C57Bl/6 mice (Harlan Sprague Dawley, Indianapolis, IN), 6–8 weeks of age, were cared for in accordance with standards of the Canadian Council on Animal Care, under an approved protocol of the University of Western Ontario Council on Animal Care. Mice were anesthetized using a ketamine/xylazine mixture (1.6 mg of ketamine and 0.08 mg of xylazine per 15 g of body mass) administered by i.p. injection. A small incision was made in the abdominal midline to expose the inferior vena cava, for injection to target the lungs. (This procedure was used to allow direct comparison with our liver studies, which require mesenteric vein injection, and to allow for videomicroscopic observation in the same studies.) A suspension of 2.5×10^5 fluorescently labeled B16F10 cells and 5×10^4 microspheres in 0.05 ml of cell culture medium was injected per mouse. Buprenorphrine analgesic (0.03 mg/kg) was given s.c. as mice awoke and also 18 h after surgery. Mice were killed at 1 h and at various times up to 14 days after injection; lungs were fixed in 10% neutral buffered formalin (pH 7.6). The surfaces of intact lung were examined by episcopic fluorescence microscopy to determine numbers of reference microspheres, solitary cells (which retain fluorescent nanospheres in the absence of cell division), and metastases, for assessment of cell survival and tumor progression (see below). Thick sections (100–150 μm) were used for analysis of overall survival and the spatial distribution of solitary cells and metastases at early time points. Thin sections (4 μm) were processed for tissue staining and quantitative stereology.

Quantification of the Time Course of Cell Survival and Metastatic Growth

To assess survival of cancer cells at any time following injection, it is necessary to compare the number of cells remaining in the tissue at any location with the number of cells originally arriving at the time of injection. This was done using our cell accounting technique (8, 9, 20). Briefly, 9-μm microspheres were mixed with the cell suspension to produce a cell:microsphere ratio of ~5:1 (the precise ratio determined by placing a drop of suspension on a coverslip and counting the numbers of cells and microspheres). On injection, the cells and microspheres entered the perfused regions of the lung in that proportion and were arrested in the microcirculation. Because the microspheres are nondeformable and larger than the capillary diameter, they became trapped by size restriction and remained as permanent markers in the lung. This has been shown to be true for liver (9) and was confirmed in this study by using the number of microspheres seen in thick (100–150 μm) sections to estimate the numbers in the whole lungs at times up to 10 days after injection, and comparing these values with the numbers originally injected (data not shown). Thus, even at later times, each microsphere observed at any location in the lung represented a known number of cells originally arriving in that region.

The ratio of cells:microspheres in the injectate was compared with the ratio found later in lung tissue, based on counts of microspheres, metastases, and the fluorescent solitary cells. Solitary cells retaining strong nanosphere fluorescence at later times represent originally injected cells, which had not divided but remained dormant. Because small metastases originate primarily from single cells (21–23), we could quantify their numbers as well, in relation to the numbers of cells originally injected. Each small metastasis was counted as representing the survival of a single injected cell. The percentage survival of injected cells was calculated as (cell:microsphere ratio in lung after injection)/(cell:microsphere ratio in syringe before injection) $\times$ 100%. The survival of cancer cells, thus, could be determined at any location within the lung, on initial arrest or at any subsequent time.

Proliferation and Apoptosis in Solitary Cells and Metastases

To determine whether solitary tumor cells or cells within metastases were undergoing proliferation, apoptosis, or remaining dormant, we used immunohistochemical staining of serial sections (4 μm) from paraffin-embedded lungs. S100 (Dako Z311) was used to identify melanoma cells, Ki-67 (Novocastra NCL-Ki67-MM1) was used to assess proliferation, and the TUNEL assay was used to assess apoptosis, as described (9), with modifications: for S100, no antigen retrieval was required; primary antibody was applied overnight at room temperature (1:400 dilution); instead of using the Envision kit, a biotinylated secondary antibody (Dako E0432) was applied, followed by strepavidin-biotin peroxidase complex (Dako K0377). For Ki-67, universal blocking solution (Dako CD310081) replaced normal goat serum. Verhoeff's iron hematoxylin elastin stain (24), which stains elastic fibers and nuclei black, collagen red, muscle and RBCs yellow, and cytoplasm gray, was used to identify vascular channels and other anatomical structures within lung sections.

At selected time points, we examined serial sections from the lungs of at least two mice. Melanoma cells were first identified in the section stained with S100. These same cells were then assessed in adjacent serial sections for markers of proliferation and apoptosis. Percentages of melanoma cells staining for Ki-67 or TUNEL were determined for: (*a*) solitary cells within the tissue; and (*b*) cells within metastases of three size ranges: <80, 80–300, and >300 μm in diameter.

Distribution of Cell Survival and Tumor Growth Relative to Lung Structures

Quantification of the distribution of tumor cells, small metastases, and macroscopic tumors in relation to the lung surface and major structures (arteries, veins, and bronchioles) in the interior was carried out using two approaches. The first, using thick tissue sections (100–150 μm), assessed the earlier stages of metastatic progression, while the location of cells and small tumors could still be represented as points. The second, using thin (4 μm) paraffin-embedded sections, was appropriate for later stages when tumors had grown irregularly through the tissue (days 10–14) and could no longer be treated as points for assessing their proximity to lung structures.

Early Stages of Tumor Progression. The aim of this approach was to determine the location of accounting microspheres, individual tumor cells, and developing tumors, with respect to the lung surface and major interior structures (arteries, veins, and bronchioles of diameter $\geq$100 μm) at successive times after cell injection. The distances of the microspheres/cells/metastases from the borders of the lung structures were computed from digitized images of entire lung sections.

After fixation, the upper lobe from the right lung of each animal was cut in half longitudinally and the lateral portion was mounted on the cut-face for preparation of 100–150-μm thick sections (Vibratome Series 1000; Technical Products International, St. Louis, MO). Sections taken from at least 1-mm deep within the lung were viewed immersed in saline using an inverted microscope. Epifluorescent illumination allowed visualization of fluorescent cells and microspheres throughout the entire thickness of the section, whereas oblique transillumination provided identification of internal structures. Each field of view was digitally captured, and overlapping fields covering the entire lung section were combined using Adobe Photoshop 5.0 (Adobe Systems Inc., San Jose, CA). In this way, when using the $\times$10 objective, a complete image of each section could be produced based on ~100 fields, at a scale of ~1 pixel/μm.

Superimposed on these images, the central positions of all microspheres,

cancer cells, and metastases were marked, based on direct visual confirmation through the microscope, and treated as points. In addition, perimeters of arteries, veins, bronchioles, and the lung surface were marked on the image. The image coordinates of the points and outlines of the lung features were used to compute the distribution of distances of microspheres, cells, and metastases from the lung surface and the surface of each interior structure. Points (microspheres, cells, or small tumors) that were within 100 μm of a lung structure were considered to be "near" it. Points that fell within 100 μm of more than one lung structure were considered "near" the closest. For comparison, the analysis was also performed on a computer-generated uniform array of points superimposed on the image of each lung section to determine the proportion of points that would be expected near any particular lung structure based on a nonpreferential distribution. In this way, all points were classified as being within one of five regions: near the lung surface, arteries, veins, or bronchioles, or within the remaining tissue.

To test for nonrandom regional distribution of blood flow at the time of injection and, therefore, preferential delivery of the cancer cells within the lung, the proportion of microspheres near each of the lung structures was compared with the proportion of uniformly spaced computer-generated points in the same region. Similarly, the survival of individual cells within each region and the formation of multicellular foci were assessed.

Later Stages of Tumor Progression. At early time points, the locations of cells, microspheres, and multicellular foci are best treated as points for analytical purposes, but once the tumors become large, proximity to anatomical structures cannot be analyzed in the same way. For example, as a tumor grows at the lung surface, its center becomes more distant from that surface. For this reason, the degree of confluence between tumor tissue and specific lung structures, as measured from thin sections, was used to quantify preferential growth, as described below.

The proportion of lung volume occupied by tumor tissue (tumor burden) immediately adjacent to the lung surface and major internal structures was compared with the overall tumor burden for the whole lung. Verhoeff's stained thin sections of lung were used to identify arteries, veins, bronchioles, and tumor tissue. Digitized composite images based on ~100 fields of view at ×10 were obtained for sections of entire lobes. The lung surface, internal structures, and regions of tumor tissue were identified and outlined on the computer images. From these images, the proportion of lung volume occupied by tumor tissue was calculated by stereological analysis. [Stereology is a well established technique commonly used in quantitative morphological studies for obtaining 3-D information from 2-D sections (25). A good explanation of the principles underlying stereological analysis is given in Howard and Reed's (26) short text, recently published in association with the Royal Microscopical Society.] Briefly, tumor burden was estimated using the Delesse principle (25, 26), which states that, on average, the volume ratio (V_V) of any component within a reference volume (*e.g.*, tumor within lung tissue) is equal to the area ratio (A_A) of that component exposed in random sections (*e.g.*, the total area of tumor profiles relative to the overall area of the lung section). For example, if the total section area was 50 mm^2 and tumors covered 10 mm^2, then 20% of the lung volume would be occupied by tumor.

Tumor burden can also be calculated from L_L, the proportion of the total length of randomly placed test lines, superimposed on the lung section, that falls on tumor tissue (25, 26). In this study, to test for preferential tumor growth at the lung surface, arteries, veins, or bronchioles, the outlines of these structures as seen in the sections were used as test lines to calculate tumor burden at those locations. For each of these structures the proportion of the overall outline length in contact with tumor tissue was then used to calculate L_L, representing the tumor burden adjacent to that structure. For example, if 50% of the outline of arteries were in contact with tumor tissue, then 50% of the volume of the tissue immediately adjacent to arteries would be tumor. For random tumor growth, V_V in the region bordering structures would be the same as V_V for the whole lung. Thus, comparison of tumor burden adjacent to the surfaces of each of the structures (L_L) with that for the whole lung (A_A) provided an index of preferential growth at the structure surfaces.

RESULTS

Cell Survival and Growth Over Time. Counts of solitary cells and metastases were expressed relative to the absolute number of cancer cells injected, rather than number of cells remaining at any given time in the tissue. This was made possible by including reference microspheres with the cell suspension injected. Cells and microspheres became arrested in vessels by size restriction, the microspheres remaining there indefinitely but the cells extravasating into the surrounding tissue. Comparison of the predicted and measured microsphere density in lung tissue at times up to 14 days after injection indicated that microspheres were not lost over this period (data not shown). Histological sections taken at 4 days after cell injection showed no evidence of cancer cells or multicellular foci, located within arterial or venous vessels. As an example, Fig. 1 shows that cells can clearly be identified as having extravasated. Survival values for fluorescent solitary cells showed a slow initial decline from 98% at 1 h to 74% by day 3, a rapid decline to 25% by day 4, followed by a relatively steady decline to 3.5% by days 12–14 (Fig. 2). In addition, counts of multicellular foci [which develop from a subset of individual injected cells (21–23)] contributed an additional 8% to the overall calculation of survival at day 4 and ~14% by days 6–8 and thereafter.

Progression of metastases through different size categories was assessed (Fig. 3). The small category included the majority of metastases found at days 4–8, but only a small proportion of those present by days 12–14. Concurrently, medium and large categories included an increasing proportion of metastases with time, accounting for the majority of those lost from the small category. Thus, once micrometastases had formed, their efficiency of progression to larger tumors was high.

We then assessed what proportions of the solitary cells or the total numbers of metastases of various sizes showed evidence of apoptosis or proliferation. We found that only ~3% of solitary cells were proliferating (Ki-67 positive) and none stained for apoptosis, indicating that most solitary cells were dormant. Most small and all medium and large metastases showed staining for proliferation; regardless of size, ~40% of cells within each metastasis stained positively. No small metastases, but 20% and 80% of medium and large metastases, respectively, showed some staining for apoptosis; for all sizes, this involved only 1–10 cells per metastasis. Whereas this would represent an estimated rate of apoptosis of about 1% of the cells in the larger tumors at later times, at day 4 apoptosis was not detected.

Regional Variation in Metastatic Progression

To characterize the location dependence of metastatic progression in the lung and to determine when such dependence became evident, we quantified the distribution of tumor cells, small metastases, and macroscopic tumors in relation to the lung surface and major structures within the interior, at successive times after cell injection.

Initial Distribution of Cells. We first determined whether injected cells were preferentially distributed in relation to structures within the

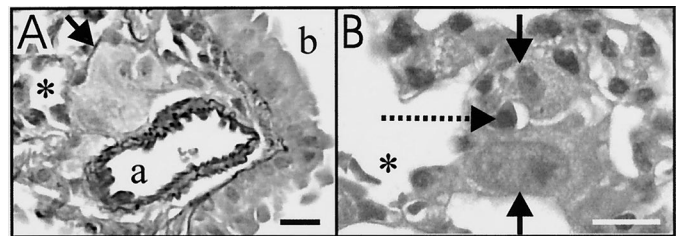

Fig. 1. Extravasated B16F10 melanoma cells in mouse lung after venous injection (4-μm thick sections; *bars*, 15 μm). *A*, Verhoeff's stain clearly shows elastin layers around arteriole (*a*) adjacent to bronchiole (*b*), 4 days after injection. Melanoma cells (*arrow*, confirmed by S100 staining in adjacent sections) in tissue between arteriole and alveolar space (*). *B*, H&E stain shows melanoma cells (*solid arrows*) surrounding capillary containing RBCs (*broken arrow*), 1 day after injection, indicating that cells were extravascular. *, alveolar space.

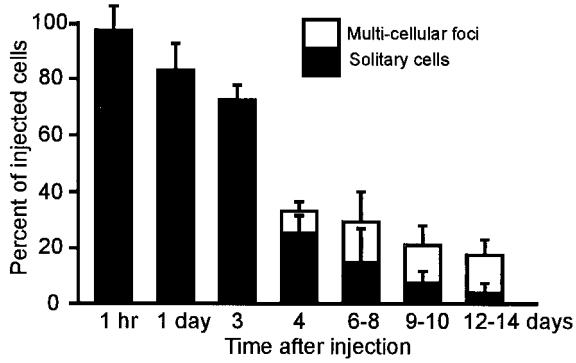

Fig. 2. Percentage of B16F10 melanoma cells, at various times after injection to target mouse lung, surviving as solitary cells or multicellular foci (*bars*, SD; n = 1, 7, 5, 3, 12, 8, and 8 mice).

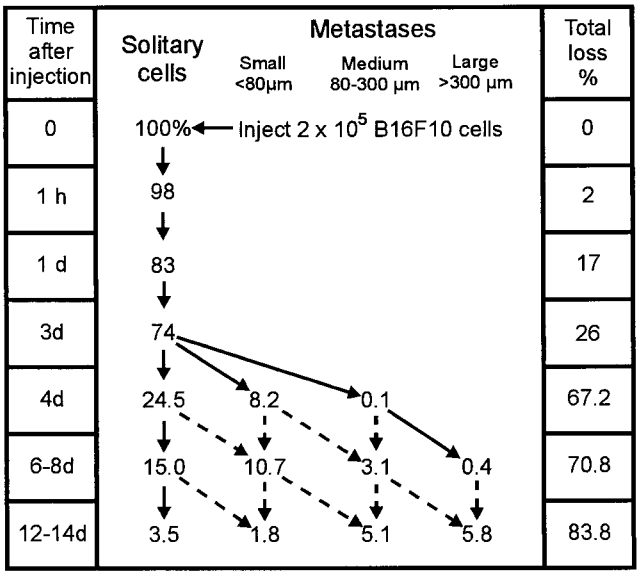

Fig. 3. Flow chart summarizing metastatic progression of B16F10 cells up to 14 days after injection to target lung, demonstrating the sequence of cell loss contributing to metastatic inefficiency. *Middle*, survival either as individual cells or as metastases of progressive sizes; *broken arrows*, some of the possible alternatives for metastatic development; *right*, progressive total loss.

lung. This distribution was quantified by recording the positions of the microspheres, which were injected along with the cells in a known ratio and became trapped indefinitely in the pulmonary microvasculature. Because microspheres and cells are both distributed by the blood flow to various regions of a lung in similar proportions, the distribution of microspheres at any time represents the initial distribution of cells. Although the greatest number of microspheres was arrested in the vicinity of arteries, this region comprised the greatest proportion of the lung volume, and blood flow per unit volume of tissue did not differ among regions. The results indicate that the delivery of cancer cells by the blood flow to different regions of the lung was in proportion to the volumes occupied by those regions (Fig. 4, □ and ■).

Early Cell Survival and Initial Cell Division. We next asked whether there was a regional dependence of cell survival or cell proliferation within the first few days after injection. We assessed the initial distributions of arrested cells (based on microsphere counts), surviving solitary cells, and micrometastases (two to four cell foci) relative to the lung volume available within each of the regions. The results for day 4 (Fig. 4) indicate that within each region distributions of solitary cells and micrometastases were almost identical to the initial cell distribution. In turn, initial cell distribution did not differ significantly from the distribution of available lung volume. This result indicates that survival and growth of injected cells at day 4 were not affected by location within the lung.

Growth of Tumor Tissue Relative to Lung Structures. We then asked whether continued tumor growth occurred preferentially at the lung surface and/or adjacent to specific structures within the lung. This possibility was tested by calculating the tumor burden adjacent to those structures, relative to the tumor burden found for the whole lung. At day 10, when the overall tumor burden was <40%, there had been preferential growth at the lung surface where there was over 80% coverage. At day 14, the difference was less pronounced (~55% *versus* ~95%), simply because there was little room left at the surface for tumor expansion. For each of the lung structures examined, Fig. 5 shows the tumor burden relative to that for whole lung. At day 10, relative tumor burden was greater for arteries, veins, and lung surface than for the whole organ (indicated by unity). However, by day 14, relative burdens for some structures tended to decrease because the tumor burden adjacent to them was already approaching 100%, whereas that for the whole lung continued to increase. (Regions such as alveoli, which are largely removed from these structures necessarily, carried a lower burden than that averaged over the entire organ.) At both times, tumor burden at the surface of the bronchioles was similar to that found throughout the lung, indicating that these structures were not supportive of preferential growth.

DISCUSSION

This study has demonstrated a high efficiency of survival of injected B16F10 cells in lung over the first 3 days following injection,

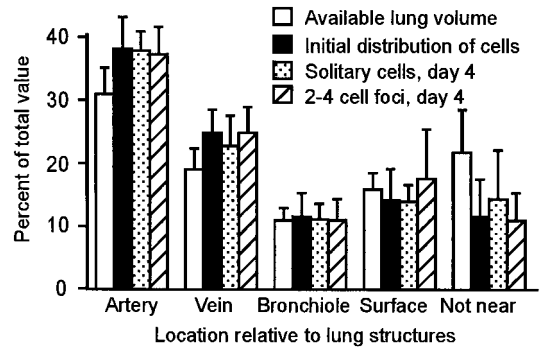

Fig. 4. Distributions of available lung volume, arrested cells immediately after injection, solitary cells at day 4, and multicellular foci at day 4 (n = 3 mice; *bars*, SE). There is no significant difference among the distributions within any region.

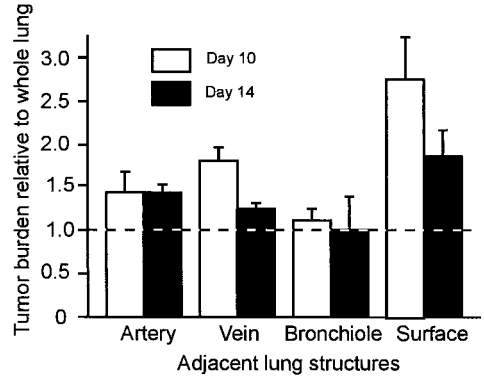

Fig. 5. Tumor burden at lung structures relative to average for whole lung section (*horizontal line* at unity) at days 10 and 14 (n = 3 mice each day; *bars*, SE). For days 10 and 14 combined, differences from unity were significant for arteries, veins, and the lung surface ($P < 0.05$).

which indicates that hemodynamic destruction of cells after arrest in the microcirculation (5) was not a major factor in these experiments. Verhoeff's elastin stain permitted resolution of arterioles and venules and location of cancer cells relative to these structures. Our results indicate a high efficiency of cell survival in the circulation, as well as a high early survival of solitary cells at extravascular locations within the lung, confirming what has been found in other organs (8–10, 19, 27). Most of these solitary cells were found to be in a dormant state. The first appearance of metastases (day 4) was accompanied by a steep decline in the numbers of solitary cells present in the tissue. Thereafter, the proportion of solitary cells gradually decreased, whereas metastases showed an initial increase in number and then simply increased in size, their cells showing negligible rates of apoptosis and high rates of proliferation. These findings suggest the possibility that dividing solitary cells may be especially vulnerable to destruction by host defenses, in contrast to metastases that continue to grow. The B16F10 melanoma cell line was selected originally, based on end point analysis, for its ability to form metastases preferentially in the lung (28). In our experiments, 16% of injected B16F10 cells were still present in the tissue 2 weeks later, either as solitary cells or metastases.

A location dependence of metastatic progression in lung has been identified previously for murine fibrosarcoma (15) and B16F10 melanoma (16, 17) cells. Thus, end point analysis has shown preferential development of metastases at the organ surface, although the initial distribution of arrested cells throughout the organ appeared to be uniform. Our goal was to quantify the time course and location dependence of growth of arrested cells, to determine at which stage in metastasis the preferential distribution of metastases became apparent. We found that the initial distribution of cells, with respect to the surface and internal structures, was random. The agreement between microsphere distribution and available lung volume for each separate structure demonstrated the uniformity of blood flow and, thus, uniformity of cancer cell delivery throughout the lung. At day 4, when extravasation was complete and small multicellular foci were first observed, both surviving solitary cells and metastases were distributed in the region of each lung structure in accordance with the associated volumes of tissue available. We, therefore, conclude that cancer cell deposition within the lung, survival of solitary cells after extravasation, and the initiation of cell division and formation of small multicellular foci are all location-independent processes.

Once metastases start to grow, however, proximity to the surface of major structures in the lung does have an influence on metastatic development. Continued random growth of randomly distributed micrometastases would form areas of contact with these major structures in proportion to their total surface areas and to the overall tumor growth in the organ. On the other hand, if growth were promoted at the surface of a particular structure, the proportion of that surface contacted by the tumor tissue would exceed the overall proportion of the lung volume occupied by tumors (25). By determining the tumor burden at specific surfaces relative to the overall tumor burden of the lung, we have documented preferential tumor growth in the tissue immediately adjacent to arterial and venous vessels and, dramatically, next to the pleural surface. With continued development and growth of tumors, however, there tended to be less relative tumor burden adjacent to veins and the lung surface, as the available space at these locations became filled.

Our previous studies in other organs have indicated that cancer cells can be relatively efficient at early steps in hematogenous metastasis. Cells are carried to secondary sites, based on patterns of blood flow, where cells arrest by size restriction, based on the relative sizes of the cells and the microvasculature in that organ. Once cells have arrested, extravasation from the circulation into the tissue seems not to be rate limiting. Cells of high and low metastatic ability, and even nonmalignant cells, may extravasate equally well and with similar kinetics (8, 10, 11, 14, 27, 29). Quantitative assessment of cell loss suggests that the metastatic process to this point is quite efficient (8, 9). These conclusions were based on experiments with a variety of cell types (melanoma, mammary carcinoma, fibroblast, and rhabdomyosarcoma) in either chick embryo CAM or mouse liver. A key aspect of the present study is its demonstration that the above conclusions apply also in the lung, thus supporting the possibility that they may be of general validity throughout the body. Indeed, we showed earlier (19) that initial cell arrest and survival in the microcirculation of skeletal muscle corresponds closely to that seen in liver.

Our measurements of percentage survival of cancer cells during metastatic progression in liver and lung, from immediately after injection until 2 weeks later, show that growth of extravasated cells in target organs is considerably less efficient, and more variable, than earlier steps in the process (*i.e.*, survival in the circulation, arrest, and extravasation). This study and our previous analysis of metastatic inefficiency in liver (9) have identified two important variables that can contribute to metastatic outcome: the proportions of cells that (*a*) initiate growth after extravasation, and (*b*) persist in growth to form metastases. However, we have found that these proportions differ markedly between B16F10 cells in lung and B16F1 cells in liver, resulting in dramatic differences in metastatic efficiency (>0.1 *versus* 0.0002). Understanding how the temporal and spatial interplay between cellular ("seed") and environmental ("soil") factors affect metastatic development will be important for understanding metastatic inefficiency and for development of therapies to combat metastasis (30, 31). Regulation of growth of cancer cells after they have extravasated offers an attractive and broad therapeutic target, and growth inhibition may be achievable by many strategies, including direct inhibition of cancer cell growth as well as control of tumor angiogenesis.

ACKNOWLEDGMENTS

We thank Kathryn Marshall for helpful assistance and discussions.

REFERENCES

1. Weinstat-Saslow, D., and Steeg, P. S. Angiogenesis and colonization in the tumor metastatic process: basic and applied advances. FASEB J., *8:* 401–407, 1994.
2. Fidler, I. J., and Ellis, L. M. The implications of angiogenesis for the biology and therapy of cancer metastasis. Cell, *79:* 185–188, 1994.
3. Liotta, L. A., and Stetler-Stevenson, W. G. Principles of molecular cell biology of cancer: cancer metastasis. *In:* V. T. DeVita Jr., S. Hellman, and S. A. Rosenberg (eds.), Cancer: Principles and Practice of Oncology, pp. 134–149. Philadelphia: J. B. Lippincott, 1993.
4. Weiss, L. Metastatic inefficiency. Adv. Cancer Res., *54:* 159–211, 1990.
5. Weiss, L. The biomechanics of cancer cell traffic, arrest, and intravascular destruction. *In:* F. W. Orr, M. R. Buchanan, and L. Weiss (eds.), Microcirculation in Cancer Metastasis, pp. 131–144. Boca Raton, FL: CRC Press, 1991.
6. Hanna, N. Role of natural killer cells in control of cancer metastasis. Cancer Metastasis Rev., *1:* 45–64, 1982.
7. Key, M. Macrophages in cancer metastasis and their relevance to metastatic growth. Cancer Metastasis Rev., *2:* 75–88, 1983.
8. Koop, S., MacDonald, I. C., Luzzi, K., Schmidt, E. E., Morris, V. L., Grattan, M., Khokha, R., Chambers, A. F., and Groom, A. C. Fate of melanoma cells entering the microcirculation: over 80% survive and extravasate. Cancer Res., *55:* 2520–2523, 1995.
9. Luzzi, K. J., MacDonald, I. C., Schmidt, E. E., Kerkvliet, N., Morris, V. L., Chambers, A. F., and Groom, A. C. Multistep nature of metastatic inefficiency: dormancy of solitary cells after successful extravasation, and limited survival of early micrometastases. Am. J. Pathol., *153:* 865–873, 1998.
10. Morris, V. L., Koop, S., MacDonald, I. C., Schmidt, E. E., Grattan, M., Percy, D., Chambers, A. F., and Groom, A. C. Mammary carcinoma cell lines of high and low metastatic potential differ not in extravasation but in subsequent migration and growth. Clin. Exp. Metastasis, *12:* 357–367, 1994.
11. Hangan, D., Uniyal, S., Morris, V. L., MacDonald, I. C., von Ballestrem, C., Thu, C., Schmidt, E. E., Chambers, A. F., Groom, A. C., and Chan, B. M. C. Integrin VLA-2 (α 2β1) function in postextravasation movement of human rhabdomyosarcoma RD cells in the liver. Cancer Res., *56:* 3142–3149, 1996.

12. Naumov, G. N., Wilson, S. M., MacDonald, I. C., Schmidt, E. E., Morris, V. L., Groom, A. C., Hoffman, R. M., and Chambers, A. F. Cellular expression of green fluorescent protein, coupled with high-resolution *in vivo* videomicroscopy, to monitor steps in tumor metastasis. J. Cell Sci., *112:* 1835–1842, 1999.
13. MacDonald, I. C., Schmidt, E. E., Morris, V. L., Chambers, A. F., and Groom, A. C. Intravital videomicroscopy of the chorioallantoic microcirculation: a model system for studying metastasis. Microvasc. Res., *44:* 185–199, 1992.
14. Koop, S., Schmidt, E. E., MacDonald, I. C., Morris, V. L., Khokha, R., Grattan, M., Leone, J., Chambers, A. F., and Groom, A. C. Independence of metastatic ability and extravasation: metastatic *ras*-transformed and control fibroblasts extravasate equally well. Proc. Natl. Acad. Sci. USA, *93:* 11080–11084, 1996.
15. Orr, F. W., Young, L., King, G. M., and Adamson, I. Y. Preferential growth of metastatic tumors at the pleural surface of mouse lung. Clin. Exp. Metastasis, *6:* 221–232, 1988.
16. Dingemans, K. P., van Spronsen, R., and Thunnissen, E. B16 melanoma metastases in mouse liver and lung. I. Location. Invasion Metastasis, *5:* 50–60, 1985.
17. Dingemans, K. P. B16 metastasis in mouse liver and lung. II. Morphology. Invasion Metastasis, *8:* 87–102, 1988.
18. Weiss, L. Comments on hematogenous metastatic patterns in humans as revealed by autopsy. Clin. Exp. Metastasis, *10:* 191–199, 1992.
19. Morris, V. L., MacDonald, I. C., Koop, S., Schmidt, E. E., Chambers, A. F., and Groom, A. C. Early interactions of cancer cells with the microvasculature in mouse liver and muscle during hematogenous metastasis: videomicroscopic analysis. Clin. Exp. Metastasis, *11:* 377–390, 1993.
20. Chambers, A. F., MacDonald, I. C., Schmidt, E. E., Morris, V. L., and Groom, A. C. Preclinical assessment of anti-cancer therapeutic strategies using *in vivo* videomicroscopy. Cancer Metastasis Rev., *17:* 263–269, 1999.
21. Talmadge, J. E., Wolman, S. R., and Fidler, I. J. Evidence for the clonal origin of spontaneous metastases. Science (Washington DC), *217:* 361–363, 1982.
22. Talmadge, J. E., and Zbar, B. Clonality of pulmonary metastases from the bladder 6 subline of the B16 melanoma studied by Southern hybridization. J. Natl. Cancer Inst., *78:* 315–320, 1987.
23. Chambers, A. F., and Wilson, S. Use of Neo^{R} B16F1 murine melanoma cells to assess clonality of experimental metastases in the immune-deficient chick embryo. Clin. Exp. Metastasis, *6:* 171–182, 1988.
24. Culling, C. F. A., Allison R. T., and Barr W. T. Cellular Pathology Technique, Ed. 4, p.175. London: Butterworths, 1985.
25. Weibel, E. R. Stereological Methods: Practical Methods for Biological Morphometry, Vol. 1, pp.26–30. London: Academic Press, 1979.
26. Howard, C. W., and Reed, M. G. Unbiased Stereology—Three-Dimensional Measurement in Microscopy. Oxford: BIOS Scientific Publishers Limited, 1998.
27. Koop, S., Khokha, R., Schmidt, E. E., MacDonald, I. C., Morris, V. L., Chambers, A. F., and Groom, A. C. Overexpression of metalloproteinase inhibitor in B16F10 cells does not affect extravasation but reduces tumor growth. Cancer Res., *54:* 4791–4797, 1994.
28. Fidler, I. J. Biological behavior of malignant melanoma cells correlated to their survival *in vivo*. Cancer Res., *35:* 218–224, 1975.
29. Chambers, A. F., MacDonald, I. C., Schmidt, E. E., Koop, S., Morris, V. L., Khokha, R., and Groom, A. C. Steps in tumor metastasis: new concepts from intravital videomicroscopy. Cancer Metastasis Rev., *14:* 279–301, 1995.
30. Poste, G., and Paruch, L. Stephen Paget, M.D., F.R.C.S. (1855–1926). A retrospective. Cancer Metastasis Rev., *8:* 93–97, 1989.
31. Radinsky, R. Modulation of tumor cell gene expression and phenotype by the organ-specific metastatic environment. Cancer Metastasis Rev., *14:* 323–338, 1995.